

Microwave-assisted one-pot synthesis of highly luminescent N-doped carbon dots for cellular imaging and multi-ion probing

Qi Xiao¹ · Yu Liang¹ · Fawei Zhu¹ · Shuangyan Lu¹ · Shan Huang¹

Received: 13 November 2016 / Accepted: 2 April 2017 / Published online: 12 April 2017
© Springer-Verlag Wien 2017

Abstract The authors report on the microwave-assisted one-step synthesis of nitrogen-doped carbon dots (N-CDs) having a fluorescence quantum yield of 80% and a fluorescence lifetime of 15.0 ns. Citric acid and ethylenediamine were used as carbon source and as a nitrogen source, respectively. The N-CDs show excellent photostability over a wide range of pH values (4–11), even at high ion strength (2 M KCl) and after 4 h of continuous UV light irradiation. This makes these N-QDs promising candidates for fluorescent probes. Cellular toxicity test showed the N-CDs not to be cytotoxic to human nasopharyngeal carcinoma cells and human embryonic kidney cells even at 400 $\mu\text{g}\cdot\text{mL}^{-1}$ levels after 48 h incubation. The fluorescence intensity of N-CDs at 445 nm is quenched by Fe(III), Hg(II), and chlorite ions, respectively. The N-CDs are shown to be viable fluorescent probes for the ions Fe(III), Hg(II), and chlorite. Respective detection limits are 12 nM, 0.8 nM, and 35 nM.

Keywords Time-resolved fluorescence · Quenching · Quantum yield · Fluorescence lifetime · High-resolution

Electronic supplementary material The online version of this article (doi:10.1007/s00604-017-2242-z) contains supplementary material, which is available to authorized users.

✉ Shan Huang
huangs@whu.edu.cn

¹ College of Chemistry and Materials Science, Guangxi Teachers Education University, Nanning 530001, People's Republic of China

transmission electron microscopy · FTIR · Stern-Volmer plot · Cell imaging · Ion analysis · Cytotoxicity

Introduction

Nitrogen-doped carbon dots (N-CDs) have attracted great attention because N-doping modulates surface defects and enhances the photoluminescence of carbon dots (CDs) [1–3]. Many methods have been explored to prepare fluorescent N-CDs, such as ultrasonic assistance [4], microplasma assistance [5], carbonization [6], and hydrothermal method [7, 8], which are classified into top-down and bottom-up routes. The majority of aforementioned methods suffer from the application of harsh synthesis conditions, tedious processes, expensive devices, and relatively low quantum yield (QY) of carbon nanodots. Therefore, it is still a great challenge to achieve cost-efficient, large-scale synthesis and high QY in one strategy.

Microwave-assisted techniques, which can provide simultaneous, homogeneous, efficient and rapid heating, and lead to faster reaction rates without high temperature and high pressure, are widely used to synthesize fluorescent carbon-based nanoparticles with highly uniform size distributions and high QYs [9–12]. Microwave-assisted methods have been reported to be used for N-CDs synthesis [13–15]. Unfortunately, the QYs of these N-CDs are relatively low compared with some commercial semiconductor quantum dots. Zhang et al. reported a one-step microwave synthesis of N-CDs with QYs of higher than 90% by using citric acid (CA) as carbon source and tris(hydroxylmethyl)aminomethane and ethanolamine as nitrogen sources [16]. However, the majority of this microwave-assisted method suffers from the application of several heating periods, complicated processes, and relatively high power of

350 W. Therefore, cost-efficient microwave-assisted strategies for the synthesis of N-CDs with high QYs are greatly needed.

Herein, a microwave-assisted method for the synthesis of strongly luminescent N-CDs was reported by using CA and ethylenediamine (EDA) as carbon source and nitrogen source, respectively. CA and EDA are dissolved in water and then high fluorescent N-CDs are obtained via one-step microwave heating (Scheme 1). N-CDs are dispersed spherical oxygenous carbon nanoparticles with 2.0–7.6 nm sizes. Due to the doping of nitrogen atom, these N-QDs not only possess high QY (> 80%) and longer fluorescence lifetimes (15.0 ns), but also exhibit super photostability in wide pH range solutions (4–11), high ion strength (2 M KCl), longtime UV light irradiation (4 h continuously), and excellent biocompatibility (non-cytotoxic to human nasopharyngeal carcinoma cells CNE-1 and human embryonic kidney cells HEK-293 T at 400 $\mu\text{g}\cdot\text{mL}^{-1}$ after 48 h incubation), which is of crucial importance for many biomedical applications.

Meanwhile, carbon-based nanoparticles are excellent probes for some specific targets, such as Cr(III) [17], Cr(VI) [18], Fe(III) [19, 20], Hg(II) [21, 22], and chlorite ions [23, 24]. These metal ions and anions were all detected based on the fluorescence quenching of carbon-based fluorescent probes. However, the detection limits of these ions are around micromolar level and the sensitivity of these methods for trace ions detection must be improved urgently. The synthesized N-CDs can be used to detect Fe(III), Hg(II), and chlorite ions with high sensitivity, which provides a promising opportunity to make use of highly fluorescent N-CDs as an effective ion detection platform.

Experimental details

Materials

Citric acid monohydrate and EDA were purchased from Shanghai Sinopharm Chemical Reagent Co., Ltd. (<http://en.reagent.com.cn/>). Dulbecco's modified Eagle's medium (DMEM), 3-(4,5-dimethylthiazol-2-yl)-2,5-

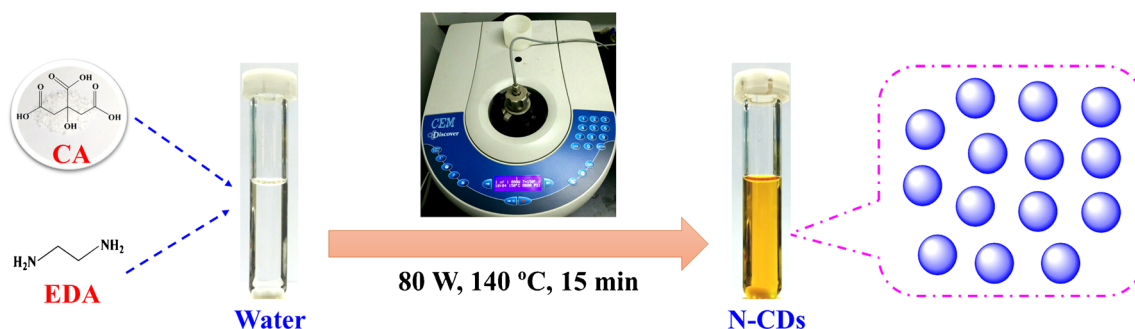
diphenyltetrazolium bromide (MTT), Roswell park memorial institute (RPMI)-1640 medium, 0.05% trypsin, fetal bovine serum (FBS) and penicillin-streptomycin solution were purchased from Shanghai Gibco Life Technologies (<http://www.thermofisher.com/cn/zh/home.html>). HEK-293 T cells and CNE-1 cells were obtained from Guangxi Medical University, China. All other chemicals were obtained from Shanghai Sinopharm Chemical Reagent Co., Ltd. (<http://en.reagent.com.cn/>). All chemicals were of the highest commercially available purity and were used as received without further purification. Ultrapure water with resistivity of 18.2 $\text{M}\Omega\cdot\text{cm}$ was prepared from a Millipore-Q Academic purification system (<http://www.merckmillipore.com/>) and was used in all experiments.

Microwave synthesis of N-CDs

Briefly, CA (0.4 M) and EDA (0.4 mL) with 5.0 mL ultrapure water were mixed uniformly under short ultrasonic vibration. The mixture was placed into microwave reaction system with relatively low power (80 W) and medium-high temperature (140 °C) for 15 min. After the reaction, the reactor was cooled to room temperature naturally and then a dark-yellow N-CDs solution was obtained (Scheme 1). The product was filtered through a 0.22 μm cellulose filter paper and then subjected to dialysis by a dialysis bag with a cut-off molecular weight of 500 Da. Viscous black solid N-CDs products were obtained by evaporating water with a rotary evaporator. Finally, the obtained N-CDs were stored at 4 °C for further applications.

Characterization of N-CDs

N-CDs were synthesized by using CEM Discover Benchmate microwave reactor (<http://cem.com/>). UV-vis absorption spectra were recorded on Agilent Cary 100 UV-vis absorption spectrophotometer (<http://www.agilent.com/home/>). Fluorescence spectra were recorded on Shimadzu RF-5301 PC luminescence spectrometer (<https://www.shimadzu.com.cn/>). Time-resolved fluorescence decay traces were captured on Horiba Jobin Yvon Fluorolog-3 system (<http://www.horiba.com/scientific/about-us/horiba-jobin-yvon/>). Fourier



Scheme 1 Schematic illustration of N-CDs synthesis

transform infrared spectroscopy (FT-IR) spectra were performed on Thermo Nicolet iS10 spectrometer (<http://www.thermofisher.com/cn/zh/home.html>). High-resolution transmission electron microscopy (HRTEM) images were recorded on JEM 2100 LaB6 high-resolution transmission electron microscope (<http://www.jeol.co.jp/en/>). Energy-dispersive X-ray spectroscopy (EDS) was captured by JEM 2100 LaB6 high-resolution transmission electron microscope equipped with AZtec TEM EDS microanalysis software (<http://www.oxford-instruments.cn/>). X-ray diffraction (XRD) was recorded on Purkinje XD-3 powder X-ray diffractometer (<http://www.pgeneral.com/>). X-ray photoelectron spectroscopy (XPS) was acquired from Perkin Elmer PHI 5000C ESCA System X-ray photoelectron spectrometer (<http://www.perkinelmer.com.cn/>). Elemental analysis was obtained using Elementar Analysensysteme Vario EL/ μ cube organic element analyzer (<http://www.elementar.de/>). MTT assay was determined by Thermo Fisher Scientific Multiskan Mk3 (<http://www.thermofisher.com/cn/zh/home.html>). Confocal fluorescence microscopy images were obtained using Nikon A1 confocal laser scanning microscope (http://www.nikon.com.cn/sc_CN/). The pH values of all solution were measured using a Sartorius PB-10 pH meter (<https://www.sartorius.com.cn/sartoriusCN/zh/CNY>).

Confocal microscopy imaging and cytotoxicity assay

HEK-293 T cells and CNE-1 cells were maintained in DMEM medium including 10% FBS and 1% penicillin-streptomycin at 37 °C in a humidified 5% CO₂ incubator. The cells were seeded onto a well plate for 24 h after the concentration reached 5×10^5 cells·mL⁻¹. Cells in exponential growth phase were used for experiment (2×10^4 cells·well⁻¹) and seeded to 96-well plates for overnight. Then, the cells were incubated with 200 μ g·mL⁻¹ N-CDs for 2 h and then washed with phosphate buffered solution three times. Finally, the imaging experiments were conducted (20 \times objective).

The cytotoxicity of N-CDs on HEK-293 T cells and CNE-1 cells was calculated by MTT assay. Firstly, HEK-293 T cells and CNE-1 cells were seeded in 96-well plates at 2×10^4 cells·well⁻¹ in DMEM medium and incubated at 37 °C in a humidified 5% CO₂ incubator. After 12 h, the cells were seeded in triplicate with fresh medium including grade concentrations of N-CDs (0, 10, 20, 50, 100, 200, and 400 μ g·mL⁻¹) at 37 °C for different times (12, 24, 36, and 48 h). Then, 20 μ L of MTT was added to each well and incubated for another 4 h. Then, the medium was removed and 200 μ L of DMSO was added to each well. The absorbance of the purple formazan at 492 nm of each well was collected using an ELISA plate reader. The cytotoxicity was calculated by the following equation: cell viability (%) = $A_1/A_2 \times 100$ (A_1 and A_2 are the absorbance of the well in which the cells were exposed or not exposed to N-CDs, respectively). Six replicate wells were

used for each control and test concentration per well. Results are expressed as their mean standard deviations.

Ion probing

In a typical detection experiment, the concentration of N-CDs was kept at 1 μ g·mL⁻¹. For Fe(III), Hg(II), and chlorite ions detection, 30 μ L of N-CDs solution (0.1 mg·mL⁻¹) and appropriate aliquot of ion solution were transferred orderly into a 5 mL Eppendorf tube. The mixture was thoroughly stirred and finally diluted to 3 mL with 0.2 M phosphate buffer (pH 7.0). The final concentrations of Fe(III) ion are 0, 0.02, 0.04, 0.06, 0.08, 0.1, 0.3, 0.5, 0.7, 1.0, 3.0, 5.0, 7.0, 9.0, 10, 20, 30, 40, 50, 70, and 90 μ M, respectively. The final concentrations of Hg(II) ion are 0, 0.01, 0.02, 0.04, 0.06, 0.08, 0.1, 0.2, 0.4, 0.6, 0.8, 1.0, 2.0, 4.0, 6.0, and 8.0 μ M, respectively. The final concentrations of chlorite ion are 0, 0.09, 0.1, 0.25, 0.4, 0.55, 0.7, 0.9, 1, 2.5, 4, 5.5, 7, 8.5, 10, 25, 40, 55, 70, 85, 100, 115, 130, 145, 160, and 310 μ M, respectively. After 3 min reaction at room temperature, the fluorescence spectra were recorded from 380 nm to 600 nm under excitation wavelength of 350 nm. The fluorescence intensity of N-CDs at 445 nm was used for quantitative analysis of three ions. The excitation slit and the emission slit were all 5 nm. The sensitivity and selectivity measurements were conducted in triplicate.

Results and discussion

Characterization of N-CDs

In this strategy, CA is selected as the carbon source for preparing N-CDs, while EDA is adopted as the source of nitrogen (Scheme 1). The fluorescent behavior of these N-CDs is affected by several factors, such as the concentration of the carbon source, the volume of the nitrogen source, the reaction temperature, the power of the microwave, and the reaction time. The experimental results show that the optimum synthesis parameters are as follows: 0.4 M CA, 400 μ L EDA, 140 °C, 80 W, and 15 min (Fig. S1 and Table S1). Such synthetic method is much faster and more convenient compared with some reported strategies for N-CDs preparation in aqueous solutions which often take several hours and need complex process.

UV-vis absorption and fluorescence spectra of N-CDs were obtained to investigate their photoluminescence property. As shown in Fig. 1a, N-CDs exhibit two typical absorption peaks from 200 nm to 420 nm. The former typical absorption peak at 238 nm is assigned to the $\pi \rightarrow \pi^*$ electronic transition of aromatic C – C bonds and the latter typical absorption peak at 345 nm is originated from the $n \rightarrow \pi^*$ electronic transitions of the C = C and C – N bonds, which is probably attributed to the formation of excited defect surface states induced by N heteroatoms [15]. Moreover, N-CDs show a very strong blue

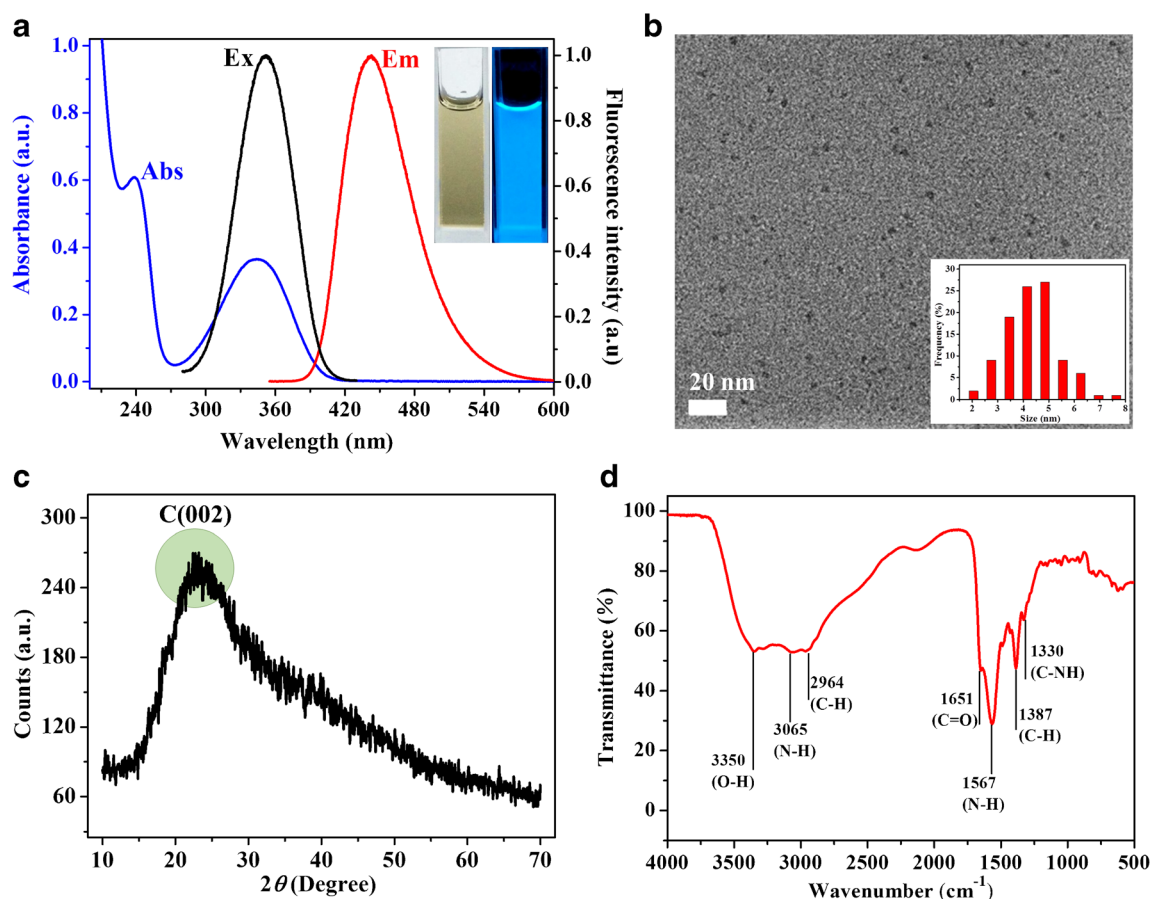


Fig. 1 **a** Normalized UV-vis absorption spectrum of N-CDs, excitation spectrum of N-CDs at $\lambda_{em} = 445$ nm and emission spectrum of N-CDs at $\lambda_{ex} = 345$ nm. Inset: Photograph of N-CDs under the radiation of white

light (Left) and 365 nm UV lamp (Right). **b** HRTEM image of N-CDs. Inset: diameter size distribution curve of N-CDs. **c** XRD pattern of N-CDs. **d** FT-IR spectrum of N-CDs

color under a hand-held UV lamp. In addition, N-CDs exhibit the same excitation wavelength-dependent band-edge fluorescence property [2, 25] (Fig. S2). The maximum excitation wavelength and the maximum fluorescence wavelength of N-CDs are 350 nm and 445 nm, respectively. Such excitation wavelength-dependent emission character is derived from the $\pi^* \rightarrow n$ electronic transitions of the surface-attached C = C and C – NH₂ bonds, which indicates that the fluorescence band can be tuned by adjusting the excitation wavelength without changing CDs. The full width at half maximum is extremely narrow (around 66 nm), which indicates that the size range of N-CDs is quite narrow.

Moreover, the average fluorescence lifetime of N-CDs is calculated to be 15.0 ns that is almost the maximum value among the reported N-CDs to our knowledge (Fig. S3). The QY of N-CDs is higher than 80% (Fig. S4). N-CDs are quite stable in wide range of pH values (4–11), high ion strength (2 M KCl) and 4 h continuous UV light irradiation (Fig. S5 to S7), which is advantageous for preservation and transportation. Dry N-CDs powder can be repeatedly re-dispersed in water without any obvious aggregation in solution, and no significant changes are observed in both UV-vis absorption

and fluorescence spectra even after 6 months storage at refrigerator. These N-CDs with super long fluorescence lifetime, relative high QY, and excellent stability can be applied directly in many biomedical regions.

HRTEM is employed to directly observe the morphology and particle size distribution of N-CDs. As shown in Fig. 1b, N-CDs have nearly spherical shapes and possess excellent solution dispersion without apparent aggregation. N-CDs exhibit narrow size distribution from 2.0 nm to 7.6 nm with an average size of 4.5 nm. As highly consistent with the reported results, N-CDs are amorphous carbon particles without any crystal lattices [26]. As exhibited in Fig. 1c, N-CDs reveal a broad peak centered at $2\theta = 24^\circ$ ($d = 0.34$ nm) which is assigned to the disordered carbon atoms with a high degree of C(002) plane for the partial graphite structure of N-CDs [27], reconfirming the amorphous carbon particles of N-CDs.

Chemical bonds and the structure of N-CDs are explored by FT-IR spectrometry. As shown in Fig. 1d, the absorption peaks of 2964 cm^{-1} and 1387 cm^{-1} are assigned to stretching vibration and bending vibration of C – H bond, respectively [15]. The broad absorption peaks at 3350 cm^{-1} and 3065 cm^{-1} are attributed to stretching vibration of O – H and N – H bonds,

respectively [10]. Two characteristic absorption peaks at 1651 cm^{-1} and 1567 cm^{-1} are ascribed to stretching vibration of C = O bond and bending vibration of N – H bond, respectively. Simultaneously, the absorption peaks at 1330 cm^{-1} and 1388 cm^{-1} are associated with bending vibration of C – N and C – H bonds, respectively [28]. Therefore, N-CDs possess abundant amide functional groups which make N-CDs are water-soluble excellently without further modification [5].

More detail information on the nature and type of constituted elements present on N-CDs can be provided through XPS technique. As shown in Fig. 2a, N-CDs show three typical characteristic peaks at 284.7 eV (C 1s), 400.5 eV (N 1s), and 534.9 eV (O 1s), respectively (Fig. S8) [16]. As exhibited in Fig. 2b, the peaks at 284.6 eV, 285.9 eV, and 288.1 eV of high-resolution C 1s spectra are corresponded to the sp^3C in C – C bond or sp^2C in C = C bond, sp^3C in C – N bond, and sp^2C in C = O bond, respectively [15], suggesting graphitic or aliphatic, nitrous, and oxygenated moieties of C 1s. High-resolution N 1s spectra also exhibit three peaks at 398.9 eV, 400.1 eV, and 401.3 eV (Fig. 2c) those are associated with N – H, N-(C)₃ and C – N – H bonds, respectively [29]. These three peaks reveal pyrrolic nitrogen and graphitic nitrogen

[15]. High-resolution O 1s spectra show two fitted peaks at 531.7 eV and 533.1 eV (Fig. 2d) those are attributed to C – O – H/C – O – C and C = O bonds, respectively [30]. XPS data demonstrate that N-CDs contain plenty of functional groups (–COOH, –OH, and N-containing groups). N-CDs show higher C content (36.76%) and O content (41.64%) but less N content (15.40%). The empirical formula for N-CDs is approximately $\text{C}_{30}\text{H}_{62}\text{N}_{11}\text{O}_{26}$ (Table S2).

Cytotoxicity of N-CDs

To demonstrate the future biomedical applications of N-CDs, the biocompatible properties of N-CDs were investigated by incubating N-CDs with CNE-1 cells and HEK-293 T cells for different times. As exhibited in Fig. 3, N-CDs are nearly non-cytotoxic to CNE-1 cells even in concentration of up to $400\text{ }\mu\text{g}\cdot\text{mL}^{-1}$ and long incubation time to 48 h (Fig. S9a). However, the cell viability decreases obviously when HEK-293 T cells are incubated with $400\text{ }\mu\text{g}\cdot\text{mL}^{-1}$ N-CDs for 24 h (Fig. S9b). When the incubation time is prolonged to 48 h, the HEK-293 T cell viability remains almost 80% of the initial value. Although N-CDs show bigger influence on HEK-293 T

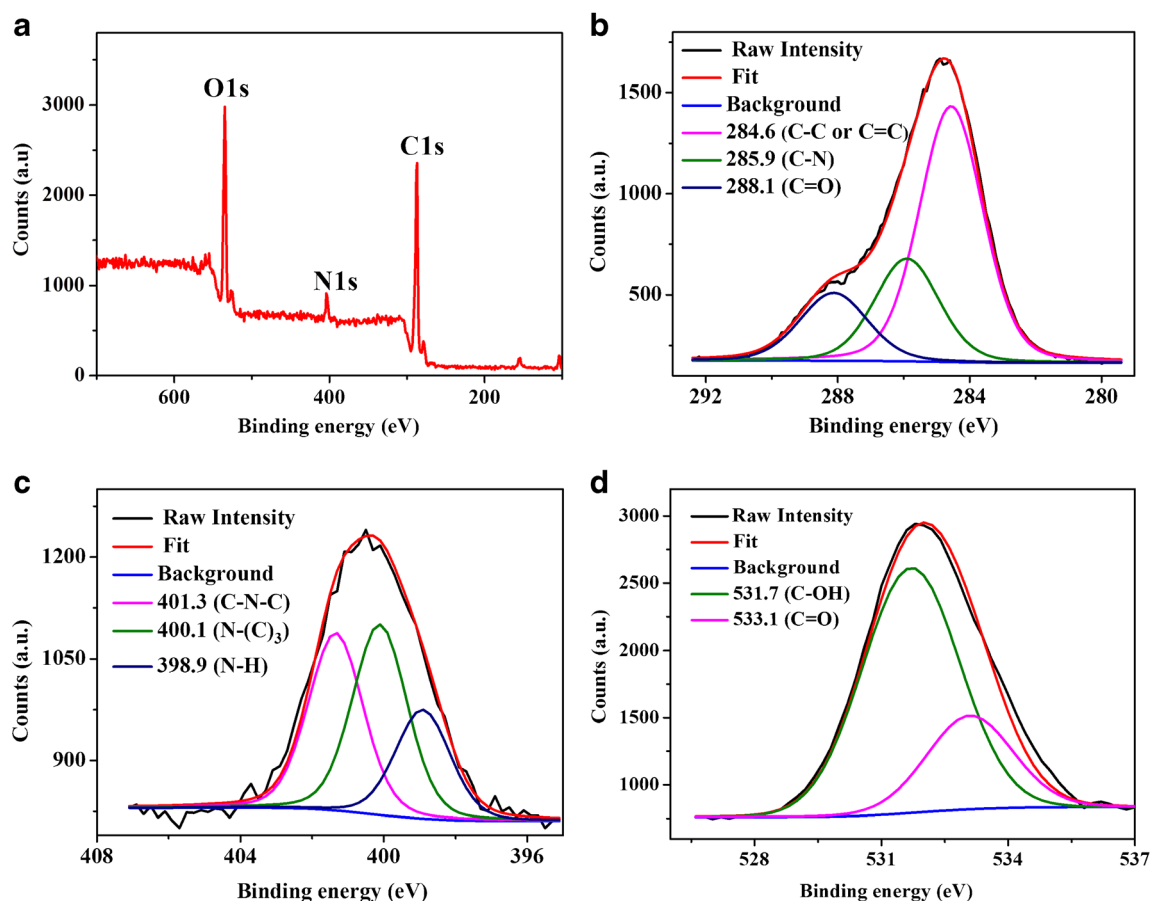


Fig. 2 a Full range XPS spectra of N-CDs. b High-resolution C 1s spectrum of N-CDs. c High-resolution N 1s spectrum of N-CDs. d High-resolution O 1s spectrum of N-CDs

cells, the cell viability change very slightly compared with the control cells as the concentrations of N-CDs increase (Fig. 3). Therefore, N-CDs exhibit excellent biomedical compatibility and can be suitable for future biomedical applications.

Cells imaging is used to expand and validate the bioimaging applications of these high QY N-CDs. CNE-1 cells and HEK-293 T cells were incubated with $200 \mu\text{g}\cdot\text{mL}^{-1}$ N-CDs solution at 37°C for 2 h. As is shown in Fig. 4, N-CDs can penetrate two cells and exhibit bright blue fluorescence inside the cells (third panels in Fig. 4). The bright-field images of two cells incubated with N-CDs (first panels in Fig. 4) indicate clearly the normal morphology of two cells, verifying that N-CDs are biocompatible and possess minimum toxicity to cells. The merged images (second panels in Fig. 4) of the first and third panels indicate the ability of N-CDs to penetrate into the cell membrane without further surface passivation. These results demonstrate that N-CDs are promising low-toxicity fluorescence staining agents for bioimaging applications. The cells display blue (third panels in Fig. 4), green (fourth panels in Fig. 4), and red (fifth panels in Fig. 4) emissions when they are excited with 405, 488, and 640 nm lasers, respectively, further demonstrating the potential of these N-CDs as multi-color bioimaging agents for

living cells. Compared with other carbon-based nanoparticles, these N-CDs are non-toxic, fairly well cell permeable, more strongly fluorescent, hardly attacked by the immunosystem, and can be used to image in the optical window of biomatter [31].

Ion probing of N-CDs

Due to the oxygen-containing groups on the surface of N-CDs, N-CDs can serve as probing candidates by coordinating with transition metal ions and some specific anions. Therefore, the fluorescence quenching effects of various metal ions on N-CDs in water solution were investigated. Different metal ions and some anions, each at a concentration of 1 mM, were added into $10 \mu\text{g}\cdot\text{mL}^{-1}$ N-CDs dispersion. As evidenced from Fig. 5, almost no obvious change in the fluorescence intensity of N-CDs can be observed except for Fe(III), Hg(II), and chlorite ions, indicating that N-CDs can be used as highly sensitive probes for the determinations of Fe(III), Hg(II), and chlorite ions. Moreover, some metal ions and anions caused relative errors of less than $\pm 5\%$ in the fluorescence intensity of N-CDs/Fe(III), N-CDs/Hg(II), or N-CDs/chlorite

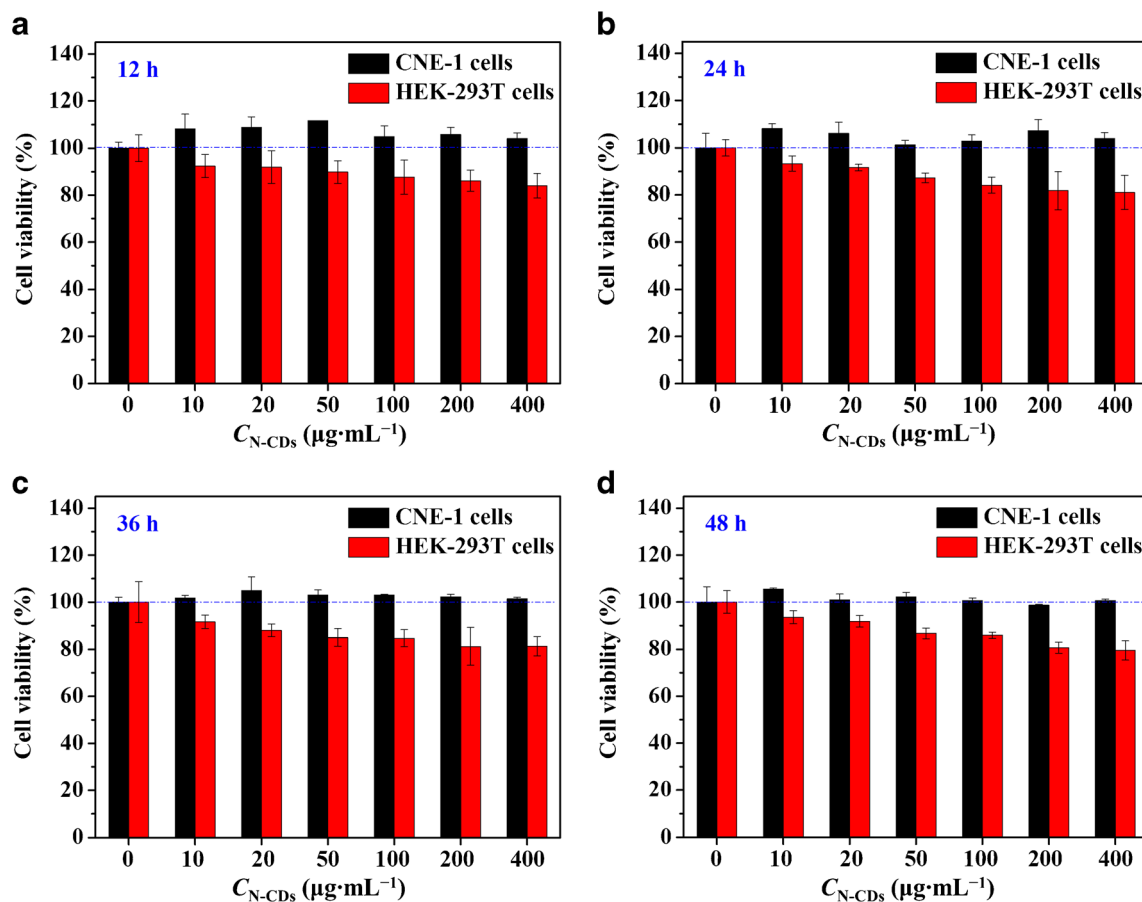


Fig. 3 Cytotoxicity investigation of N-CDs in CNE-1 cells and HEK-293 T cells. The cells are incubated with various concentrations of N-CDs ($10\text{--}400 \mu\text{g}\cdot\text{mL}^{-1}$) for 12 h (a), 24 h (b), 36 h (c), and 48 h (d) in dark.

The cell viability is normalized to the control. The cell viability is determined by MTT reduction assay and the results are expressed as the mean \pm S.D. of six separate trials

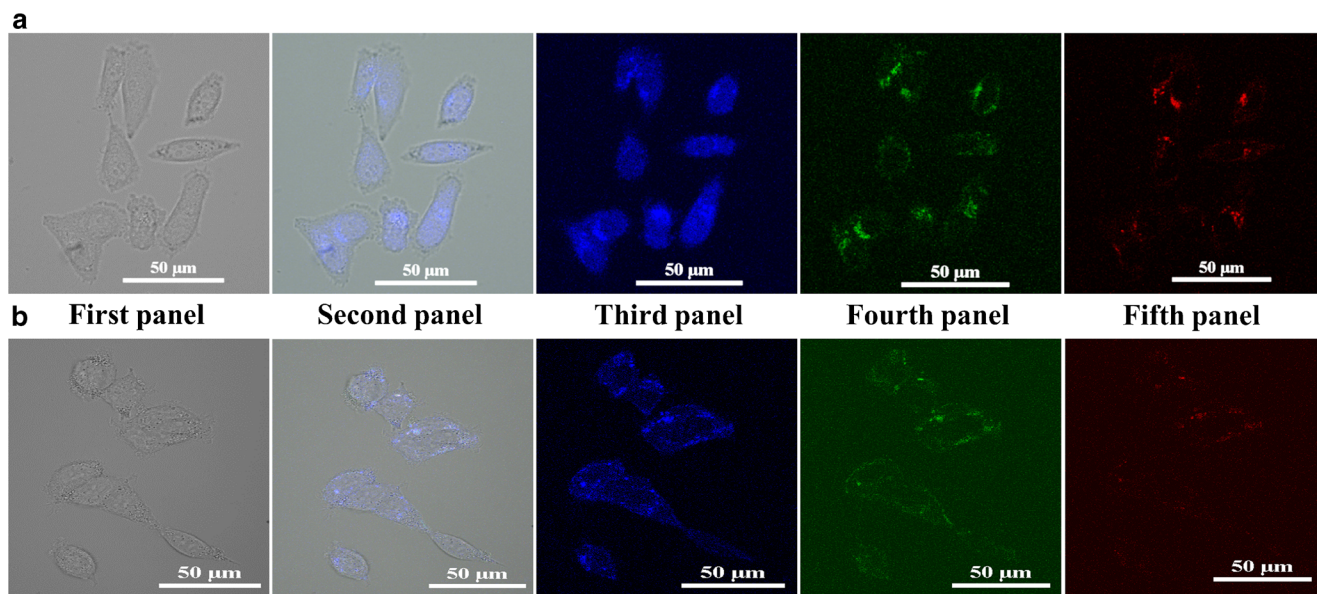


Fig. 4 Confocal fluorescence images of CNE-1 cells (a) and HEK-293 T cells (b) incubated with $200 \mu\text{g}\cdot\text{mL}^{-1}$ N-CDs at $37 \text{ }^\circ\text{C}$ for 2 h. The first left panels show the bright-field images of two cells. The second panels

are the merged images of the first and third panels. The third, fourth, and fifth panels are cell images taken at λ_{ex} of 405, 488, and 640 nm, respectively

(Table S3), suggesting that these metal ions and anions had no serious interference in the determination of three ions.

Fluorescence spectra of N-CDs under different concentrations of Fe(III), Hg(II), and chlorite ions were recorded, and the relationships between concentrations of three ions and fluorescence intensity of N-CDs were further investigated. As shown in Fig. 6, Fe(III), Hg(II), and chlorite ions efficiently quench the fluorescence of N-CDs with the increase of the concentration of three ions. The change of fluorescence intensity of N-CDs is sensitive to the concentrations of three ions, which can be described by the well-known Stern-Volmer equation: $I_0/I = 1 + K_{\text{SV}} [Q]$. Herein, K_{SV} is the Stern-Volmer quenching constant, $[Q]$ is the concentration of quencher, I_0 and I represent the fluorescence intensity of N-CDs in the absence and presence of quencher,

respectively. Three good linear relationships exist between the change of fluorescence intensity of N-CDs and the concentrations of three ions. The K_{SV} values are $19,790 \text{ L}\cdot\text{mol}^{-1}$ for Fe(III) ion, $297,540 \text{ L}\cdot\text{mol}^{-1}$ for Hg(II) ion, and $4020 \text{ L}\cdot\text{mol}^{-1}$ for chlorite ion, respectively. Based on the $3\sigma/K_{\text{SV}}$ (σ is the standard deviation of the blank signal of N-CDs), the detection limits of Fe(III), Hg(II), and chlorite ions are calculated to be 12 nM, 0.8 nM, and 35 nM, respectively, which are comparable to the sensitive approach reported (Table S4). N-CDs can be utilized to detect three ions in synthetic samples, and the values found for synthetic samples are highly identical with the spiked values (Table S5) with the recoveries of 96.5% to 103.8%.

Fluorescence quenching mechanism can be directly distinguished by investigating the variation of fluorescence

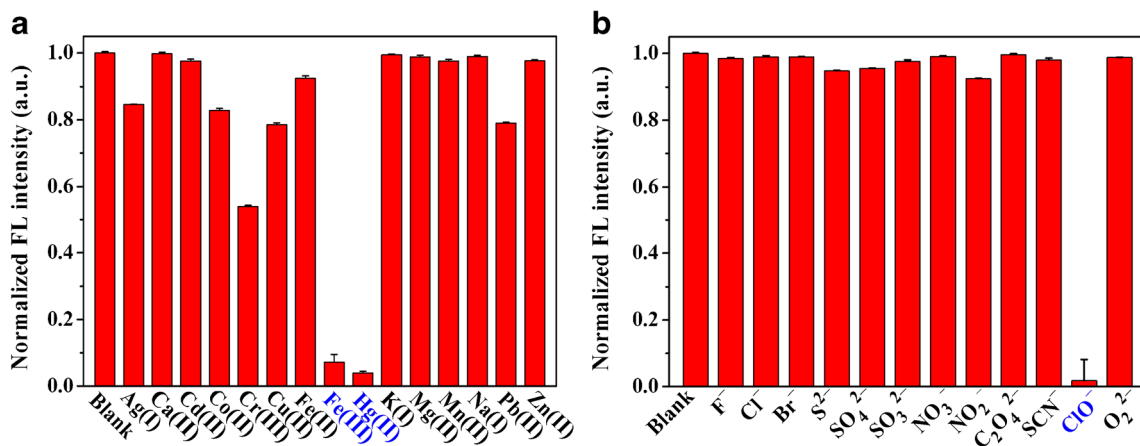


Fig. 5 Fluorescence intensity of N-CDs at 445 nm after the addition of different metal ions (a) and anions (b). The concentration of N-CDs is $10 \mu\text{g}\cdot\text{mL}^{-1}$ and the concentrations of all ions are 1 mM

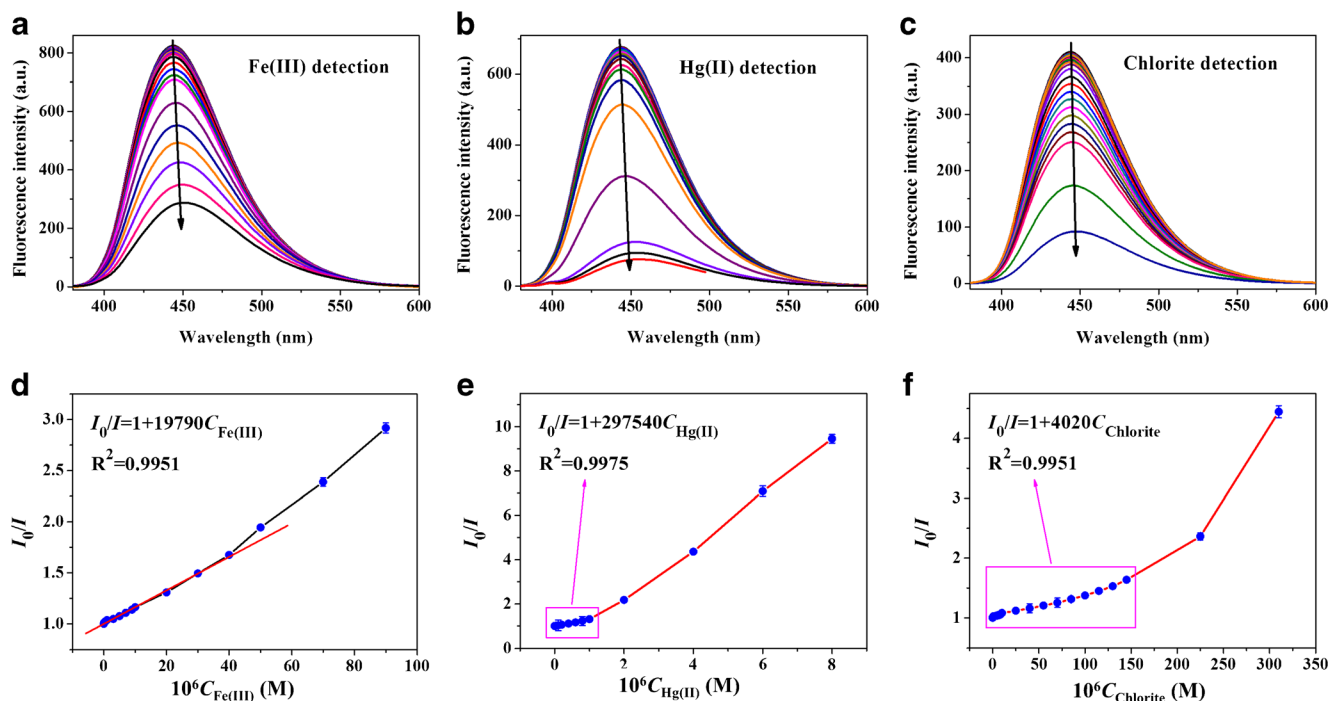


Fig. 6 **a** Fluorescence spectra of N-CDs in different concentrations of Fe(III) ion (from top to bottom): 0, 0.02, 0.04, 0.06, 0.08, 0.1, 0.3, 0.5, 0.7, 1.0, 3.0, 5.0, 7.0, 9.0, 10, 20, 30, 40, 50, 70, and 90 μM . **b** Fluorescence spectra of N-CDs in different concentrations of Hg(II) ion (from top to bottom): 0, 0.01, 0.02, 0.04, 0.06, 0.08, 0.1, 0.2, 0.4, 0.6, 0.8, 1.0, 2.0, 4.0, 6.0, and 8.0 μM . **c** Fluorescence spectra of N-CDs in different concentrations of chlorite ion (from top to bottom): 0, 0.09, 0.1, 0.25, 0.4, 0.55, 0.7, 0.9, 1, 2.5, 4, 5.5, 7, 8.5, 10, 25, 40, 55, 70, 85, 100,

115, 130, 145, 160, and 310 μM . Linear relationships between the change of fluorescence intensity of N-CDs and the concentrations of Fe(III) ion **d**, Hg(II) ion **e**, and chlorite ion **f**, respectively. The concentration of N-CDs in three experiments is remained at 1.0 $\mu\text{g}\cdot\text{mL}^{-1}$. Fluorescence spectra were recorded from 380 nm to 600 nm under excitation wavelength of 350 nm. The fluorescence intensity of N-CDs at 445 nm was used for quantitative analysis of three ions

lifetime, since fluorescence lifetime of a fluorophore usually changes in dynamic quenching process but remains constant during static quenching process [32, 33]. The fluorescence lifetime of N-CDs is shortened from 15.0 ns to about 12.6 ns, 8.8 ns, and 9.9 ns after the addition of 10 μM Fe(III) ion, 1.0 μM Hg(II) ion, and 100 μM chlorite ion, respectively (Fig. S10), suggesting the dynamic fluorescence quenching mechanism. Some literatures report that Fe(III) ion can dynamically quench the fluorescence of CDs [19], mainly because Fe(III) ion has higher thermodynamic affinity and faster chelating processes towards amide ligands of N-CDs [20]. However, unlike Fe(III) ion, Hg(II) ion often quench the fluorescence of CDs via effective electron transfer process that facilitates the non-radiative electron/hole recombination annihilation, due to the stronger affinity between Hg(II) ion and carboxy groups of N-CDs [22]. Different from these metal ions, the exact dynamic quenching mechanism of N-CDs by chlorite ion is not fully known. The surface of N-CDs contains huge amounts of reductive hydroxyl groups because of incomplete carbonization, and chlorite ion can react

with these groups through redox reaction. Therefore, chlorite ion may destroy the surface passivation of N-CDs and quench the fluorescence of N-CDs [23].

Conclusion

The synthesis of N-CDs with high QY and excellent biocompatibility through microwave-assisted approach was demonstrated. The structure of N-CDs was adequately characterized by HRTEM, FT-IR, XPS, EDS, XRD, and elemental analysis. The photoproperty of N-CDs was further investigated by UV-vis absorption spectra and fluorescence spectra. These N-CDs not only possess high QY and excellent photostability but also exhibit favorable biocompatibility and low cytotoxicity on CNE-1 cells and HEK-293 T cells, which are most important for future biological and biomedical applications. As such, these high fluorescent and good biocompatible N-CDs are further used to sensitively detect Fe(III), Hg(II), and chlorite ions with satisfied results. These N-CDs may have a broad range of desirable applications in analytical areas.

Acknowledgements This work was financially supported by National Natural Science Foundation of China (21563006, 21403039), Natural Science Foundation of Guangxi Province (2015GXNSFAA139033, 2016GXNSFBA380118), BAGUI Scholar Program of Guangxi Province of China, and Guangxi Colleges and Universities Key Laboratory of Synthetic and Natural Functional Molecular Chemistry, Guangxi Teachers Education University.

Compliance with ethical standards The author(s) declare that they have no competing interests.

References

- Tan J, Zou R, Zhang J, Li W, Zhang LQ, Yue DM (2016) Large-scale synthesis of N-doped carbon quantum dots and their phosphorescence properties in a polyurethane matrix. *Nanoscale* 8:4742–4747. doi:10.1039/c5nr08516k
- Yang YM, Kong WQ, Li H, Liu J, Yang MM, Huang H, Liu Y, Wang ZY, Wang ZQ, Sham TK, Zhong J, Wang C, Liu Z, Lee ST, Kang ZH (2015) Fluorescent N-doped carbon dots as in vitro and in vivo nanothermometer. *ACS Appl Mater Interfaces* 7:27324–27330. doi:10.1021/acsami.5b08782
- Zuo PL, Lu XH, Sun ZG, Guo YH, He H (2016) A review on syntheses, properties, characterization and bioanalytical applications of fluorescent carbon dots. *Microchim Acta* 183:519–542. doi:10.1007/s00604-015-1705-3
- Ma Z, Ming H, Huang H, Liu Y, Kang ZH (2012) One-step ultrasonic synthesis of fluorescent N-doped carbon dots from glucose and their visible-light sensitive photocatalytic ability. *New J Chem* 36:861–864. doi:10.1039/c2nj20942j
- Wang Z, Lu YX, Yuan H, Ren ZH, Xu C, Chen J (2015) Microplasma-assisted rapid synthesis of luminescent nitrogen-doped carbon dots and their application in pH sensing and uranium detection. *Nanoscale* 7:20743–20748. doi:10.1039/c5nr05804j
- Xu Y, Wu M, Liu Y, Feng XZ, Yin XB, He XW, Zhang YK (2013) Nitrogen-doped carbon dots: a facile and general preparation method, photoluminescence investigation, and imaging applications. *Chem Eur J* 19:2276–2283. doi:10.1002/chem.201203641
- Qian ZS, Ma JJ, Shan XY, Feng H, Shao LX, Chen JR (2014) Highly luminescent N-doped carbon quantum dots as an effective multifunctional fluorescence sensing platform. *Chem Eur J* 20:2254–2263. doi:10.1002/chem.201304374
- Yang Z, Xu MH, Liu Y, He FJ, Gao F, Su YJ, Wei H, Zhang YF (2014) Nitrogen-doped, carbon-rich, highly photoluminescent carbon dots from ammonium citrate. *Nanoscale* 6:1890–1895. doi:10.1039/c3nr05380f
- Hou J, Li HY, Wang L, Zhang P, Zhou TY, Ding H, Ding L (2016) Rapid microwave-assisted synthesis of molecularly imprinted polymers on carbon quantum dots for fluorescent sensing of tetracycline in milk. *Talanta* 146:34–40. doi:10.1016/j.talanta.2015.08.024
- Pedro SG, Salinas-Castillo A, Ariza-Avidad M, Lapresta-Fernández A, Sánchez-González C, Martínez-Cisneros CS, Puyol M, Capitan-Vallvey LF, Alonso-Chamarro J (2014) Microsystem-assisted synthesis of carbon dots with fluorescent and colorimetric properties for pH detection. *Nanoscale* 4:6018–6024. doi:10.1039/c4nr00573b
- Xu ZZ, Wang CX, Jiang KL, Lin HH, Huang YJ, Zhang C (2015) Microwave-assisted rapid synthesis of amphibious yellow fluorescent carbon dots as a colorimetric nanosensor for Cr(VI). *Part Part Synt Charact* 32:1058–1062. doi:10.1002/ppsc.201500172
- Zhang CF, Cui YY, Song L, Liu XF, Hu ZB (2016) Microwave assisted one-pot synthesis of graphene quantum dots as highly sensitive fluorescent probes for detection of iron ions and pH value. *Talanta* 150:54–60. doi:10.1016/j.talanta.2015.12.015
- Edison TN, Atchudan R, Sethuraman MG, Shim JJ, Lee YR (2016) Microwave assisted green synthesis of fluorescent N-doped carbon dots: cytotoxicity and bio-imaging applications. *J Photochem Photobiol B* 161:154–161. doi:10.1016/j.jphotobiol.2016.05.017
- Jiang YL, Wang YX, Meng FD, Wang BX, Cheng YX, Zhu CJ (2015) N-doped carbon dots synthesized by rapid microwave irradiation as highly fluorescent probes for Pb²⁺ detection. *New J Chem* 39:3357–3360. doi:10.1039/c5nj00170f
- Xu MH, Xu SS, Yang Z, Shu MJ, He GL, Huang D, Zhang LL, Li L, Cui DX, Zhang YF (2015) Hydrophilic and blue fluorescent N-doped carbon dots from tartaric acid and various alkylol amines under microwave irradiation. *Nanoscale* 7:15915–15923. doi:10.1039/c5nr04209g
- Zhang YQ, Liu XY, Fan Y, Guo XY, Zhou L, Lv Y, Lin J (2016) One-step microwave synthesis of N-doped hydroxyl-functionalized carbon dots with ultra-high fluorescence quantum yields. *Nanoscale* 8:15281–15287. doi:10.1039/c6nr03125k
- Chang MMF, Ginjom IR, Ngu-Schwemlein M, Ng SM (2016) Synthesis of yellow fluorescent carbon dots and their application to the determination of chromium(III) with selectivity improved by pH tuning. *Microchim Acta* 183:1899–1907. doi:10.1007/s00604-016-1819-2
- Huang S, Qiu HN, Zhu FW, Lu SY, Xiao Q (2015) Graphene quantum dots as on-off-on fluorescent probes for chromium(VI) and ascorbic acid. *Microchim Acta* 182:1723–1731. doi:10.1007/s00604-015-1508-6
- Wang FX, Hao QL, Zhang YH, Xu YJ, Lei W (2016) Fluorescence quenchometric method for determination of ferric ion using boron-doped carbon dots. *Microchim Acta* 183:273–279. doi:10.1007/s00604-015-1650-1
- Li LB, Li L, Wang C, Liu KY, Zhu RH, Qiang H, Lin YQ (2015) Synthesis of nitrogen-doped and amino acid-functionalized graphene quantum dots from glycine, and their application to the fluorometric determination of ferric ion. *Microchim Acta* 182:763–770. doi:10.1007/s00604-014-1383-6
- Tang WJ, Wang Y, Wang PP, Di JW, Yang JP, Wu Y (2016) Synthesis of strongly fluorescent carbon quantum dots modified with polyamidoamine and a triethoxysilane as quenchable fluorescent probes for mercury(II). *Microchim Acta* 183:2571–2578. doi:10.1007/s00604-016-1898-0
- Yan FY, Kong DP, Luo YM, Ye QH, He JJ, Guo XF, Chen L (2016) Carbon dots serve as an effective probe for the quantitative determination and for intracellular imaging of mercury(II). *Microchim Acta* 183:1611–1618. doi:10.1007/s00604-016-1788-5
- Lin YP, Yao BX, Huang TT, Zhang SC, Cao XT, Weng W (2016) Selective determination of free dissolved chlorine using nitrogen-doped carbon dots as a fluorescent probe. *Microchim Acta* 183:2221–2227. doi:10.1007/s00604-016-1855-y
- Simões EF, Leitão JM, da Silva JCE (2016) Carbon dots prepared from citric acid and urea as fluorescent probes for hypochlorite and peroxydinitrite. *Microchim Acta* 183:1769–1777. doi:10.1007/s00604-016-1807-6
- Sun J, Yang SW, Wang ZY, Shen H, Xu T, Sun LT, Li H, Chen WW, Jiang XY, Ding GQ, Kang ZH, Xie XM, Jiang MH (2015) Ultra-high quantum yield of graphene quantum dots: aromatic-nitrogen

- doping and photoluminescence mechanism. Part Part Syst Charact 32:434–440. doi:10.1002/ppsc.201400189
26. Zhu SJ, Meng QN, Wang L, Zhang JH, Song YB, Jin H, Zhang K, Sun HC, Wang HY, Yang B (2013) Highly photoluminescent carbon dots for multicolor patterning, sensors, and bioimaging. *Angew Chem Int Ed* 52:3953–3957. doi:10.1002/anie.201300519
 27. Liu Y, Xiao N, Gong NQ, Wang H, Shi X, Gu W, Ye L (2014) One-step microwave-assisted polyol synthesis of green luminescent carbon dots as optical nanoprobos. *Carbon* 68:258–264. doi:10.1016/j.carbon.2013.10.086
 28. Zhuo Y, Miao H, Zhong D, Zhu SS, Yang XM (2015) One-step synthesis of high quantum-yield and excitation-independent emission carbon dots for cell imaging. *Mater Lett* 139:197–200. doi:10.1016/j.matlet.2014.10.048
 29. Zou Y, Yan FY, Dai LF, Luo YM, Fu Y, Yang N, Wu JY, Chen L (2014) High photoluminescent carbon nanodots and quercetin-Al³⁺ construct a ratiometric fluorescent sensing system. *Carbon* 77:1148–1156. doi:10.1016/j.carbon.2014.06.056
 30. Wang CX, Xu ZZ, Cheng H, Lin HH, Humphrey MG, Zhang C (2015) A hydrothermal route to water-stable luminescent carbon dots as nanosensors for pH and temperature. *Carbon* 82:87–95. doi:10.1016/j.carbon.2014.10.035
 31. Wolfbeis OS (2015) An overview of nanoparticles commonly used in fluorescent bioimaging. *Chem Soc rev* 44:4743–4768. doi:10.1039/c4cs00392f
 32. Orte A, Alvarez-Pez JM, Ruedas-Rama MJ (2013) Fluorescence lifetime imaging microscopy for the detection of intracellular pH with quantum dot nanosensors. *ACS Nano* 7:6378–6395. doi:10.1021/nn402581q
 33. Lakowicz JR (2006) Principles of fluorescence spectroscopy, 3rd edn. Plenum Press, New York